Indian Journal of Geo Marine Sciences
Vol. 53 (05), May 2024, pp. 299-309
DOI: 10.56042/ijms.v53i05.21659

Oblique wave interaction with pile-restrained dual H-shaped breakwater

A Panda, D Karmakar* & M Rao

Department of Water Resources and Ocean Engineering, National Institute of Technology Karnataka, Surathkal, Mangalore, Karnataka – 575 025, India

*[E-mail: dkarmakar@nitk.edu.in]

Received 26 March 2024; revised 13 May 2024

The hydrodynamic performance of pile-restrained dual H-shaped floating breakwater is investigated using the small amplitude wave theory considering oblique wave incidence. The research on a single H-shaped floating structure supported by the piles has demonstrated effective wave reflection and wave trapping due to its distinctive configuration, composed of a vertical member called a web and a horizontal member called a flange. Thus, the dual H-shaped breakwater is proposed to enhance the breakwater's efficiency and to provide additional support to the leeside structure. The present analysis is performed by varying the structural parameters such as the width and submergence draft of the web, flange width of the dual H-shaped breakwaters and the corresponding effect on the hydrodynamic coefficients along with the wave-induced force acting horizontally on the breakwater using Multi-Domain Boundary Element Method (MDBEM). Based on the study, the leeside structure experiences a greater wave force than the primary H-shaped structure placed seaside for the critical angle of incidence. The dual H-shaped breakwater is noted as a highly effective harbour defence solution based on the structural and design specifications. The dual H-shaped pile-restrained floating breakwaters provide protection by absorbing the highest wave force and releasing a significant quantity of wave energy.

[**Keywords**: Dual breakwaters, H-shaped breakwater, Multi-Domain Boundary Element Method (MDBEM), Reflection and transmission coefficients, Wave force coefficient]

Nomenclature

a	Wave amplitude
b_w, b_f and b_p	Width of the web, flange and plates
d_w, d_f and d_p	Submergence draft of web, flange and plates measured from the free surface
f	Linearised friction coefficient for the structure
g	Acceleration due to gravity
G	Free surface Green's function
h	Depth of water
i	Imaginary unit
k	Wave number in the open water region
k_p	Pressure response factor
K_r, K_t and K_d	Reflection, transmission and dissipation coefficient
K_{fb1} and K_{fb2}	Horizontal force coefficient on the front face of the seaside and leeside breakwater of two H-shaped configurations
N	Total number of constant boundary elements
P_w	Wave-pressure coefficient
S	Coefficient of inertia for the porous structure
t	Time in seconds
T	Wave period
w_s	Width of the spacing between two adjacent breakwaters
∇	Laplace operator
Δ_x	Constant boundary element
ε	Porosity of the structure
ρ	Density of water
ω	Wave frequency
λ	Wavelength
ϕ	Velocity potential
θ	Angle of incident wave
δ	Dirac-delta function
ϕ^f, ϕ^s, ϕ_I, ϕ_R and ϕ_T	Velocity potential in the fluid, structure, incident, reflected and transmitted regions
Γ_j	Boundary in the j^{th} element

Introduction

In recent years, larger ports with deeper channels have been required to handle the increasing volume of sea trade due to the spike in maritime activity. The primary concern of the ocean and coastal engineers in the busy harbour region is the prevention of coastal erosion from the nearby region to the port channel. So, the floating breakwater has emerged as an affordable solution to reduce the nearby coastal erosion compared to the traditional rubble mound breakwaters. The ease of fabrication, transportation, and construction makes the floating breakwater advantageous even in poor seabed conditions and deep water depths. Adee[1] showed a direct correlation between incident-wave frequency and floating breakwater performance, which resulted in studying different types of floating breakwaters and installation techniques. Hales[2]

conducted numerous studies on floating breakwaters and proposed that using floating breakwaters reduces the number of ship mooring spaces close to the harbour, lowers building costs in deep-sea conditions, and offers an alternative option for weak seabed foundations for coastal protection measures. Further, Dai *et al*.[3] effectively demonstrated the evolution of research on floating breakwaters over the years, which covers a variety of structural parameters and forms of floating breakwaters.

The studies on the floating breakwaters are widely initiated to counter the inefficiency of massive submerged breakwaters under poor seabed conditions and deep water regions. Experimental studies on the wave scattering coefficients for four different types of floating structures were carried out by Kato *et al*.[4] and concluded that the configuration with easy rolling towards the incident wave has an impressive damping. A comparison of efficiency of floating and submerged obstacles revealed that the determination of hydrodynamic coefficients of rectangular barriers is effectively facilitated by the variational approach[5]. Studies on wave interaction with breakwaters includes the investigations of different submerged breakwaters[6], hydrodynamic performance of permeable absorbers[7], floating pontoon breakwater[8] and floating porous boxes[9]. In the last few decades, studies on designing innovative floating breakwaters have been performed that can replace traditional structures while reducing the structural volume and improving cost-effectiveness. The effectiveness and performance of the various floating breakwater configurations and the studies show that T-shaped breakwaters are efficient (up to 65 % dissipation)[10]. However, H-shaped structures have emerged for better wave control. Wang & Sun[11] introduced a novel design for a floating breakwater that reduces transmission and mooring force by assembling several diamond-shaped structures. Experimental research on the hydrodynamic characteristics of floating breakwater, both alone and in combination with pneumatic chambers, which can enhance energy dissipation and decrease wave transmission, was performed by He *et al*.[12]. Koraim & Rageh[13] analysed the wave interaction with floating breakwater for several different wave periods and wave heights by measuring the hydrodynamic coefficients.

In addition to this, the safety to the leeside structures is necessary for protecting the coastline and harbour areas. Extensive research on multiple floating structures was performed by Syed & Mani[14] with three rigidly interconnected pontoons of equal spacing, where the scattering coefficients are significantly affected by the inter structural spacing. Cho *et al*.[15] compared the performance of an array of rectangular and trapezoidal breakwaters experimentally and concluded that the series of trapezoidal breakwaters is more prominent for lesser areal occupation and effective reflection. Bragg resonance studies on multiple semicircular breakwaters performed by Liu *et al*.[16] proved that the model is efficient in defending against wave attack and stable against wave force through analytical and experimental studies. Study on the effect of inter-structural spacings on Bragg's scatterings by Ouyang *et al*.[17] on an array of fixed floating pontoon structures using the boundary discretisation method and by Catipovi *et al*.[18] on an array of floating breakwaters using time domain analysis concluded the usefulness of the multiple models. Analysis of a pair of floating breakwaters using the BEM approach by Vijay & Sahoo[19] suggested that the seaside structure experiences significantly higher wave force than the leeside of the structure. Additional studies on wave interaction with various structures for a set of rectangular trenches[20], multiple rectangular and triangular floating structures[21], and a series of multiple floating inverted trapezoidal porous boxes[22] have further explained the Bragg's resonance. Recently, a numerical investigation on dual-row cuboid and cylindrical floating breakwaters revealed that the dual floating breakwater is efficient in wave transmission properties when compared to single structures[23].

The literature review revealed that limited research is performed on multi-unit breakwaters with novel configurations to maximise energy dissipation. Therefore, the hydrodynamic analysis of the dual H-shaped pile-restrained floating breakwaters under the influence of oblique waves is the primary focus of the current study. The variations for wave reflection, transmission, and dissipation coefficients, along with wave force on the leeside and seaside of the structure, are analysed for the oblique wave incidence. A comparative analysis between the wave reflection characteristics and wave force coefficients is also conducted to understand the efficiency under different structural conditions.

Materials and Methods

Theoretical formulation

The small amplitude wave theory is employed to analyse the hydrodynamic performance of a dual

H-shaped breakwater system. Figure 1 illustrates the ideal geometry of dual H-shaped pile-restrained floating breakwaters that depict the different structural and physical properties and the fluid/structural boundaries. Further, the layout of the suggested dual H-shaped breakwater with matching intra-structure spacing is discussed. The numerical analysis of the oblique wave-structure interaction and the intricate mathematical process is based on MDBEM approach[24].

Since the assumed fluid flow is irrotational, incompressible and inviscid, the velocity potential for the oblique wave can be expressed as: $\phi(x,y,z,t) = Re\{\phi(x,y)e^{i(k_z-\omega t)}\}$, where $k_z = k\sin\theta$. In the fluid domain Ω, the velocity potential fulfils Helmholtz's equation, which is represented as

$$(\nabla^2 - {k_z}^2)\phi(x,y) = 0 \quad \ldots (1)$$

The fluid domain is composed of seabed boundary Γ_{SB}, boundaries for the input region Γ_{INPUT} and output region Γ_{OUTPUT} and free-surface boundary Γ_{FS}. The fluid flow is assumed to be from the negative x-axis to the positive x-axis, precisely from the incident region Γ_{INPUT} to the transmitted region Γ_{OUTPUT}. The free surface Γ_{FS} boundary condition is given by:

$$\frac{\partial\phi}{\partial y} - \frac{\omega^2}{g}\phi = 0 \quad \ldots (2)$$

The horizontal sea-bed Γ_{SB} which is assumed to be flat and impermeable, the sea-bottom boundary condition is of the form

$$\frac{\partial\phi}{\partial y} = 0 \text{ at } y = -h \quad \ldots (3)$$

The fluid areas surrounding each interface are in contact with the porous structure. Therefore, to preserve the continuity of mass flow and pressure between nearby structures and fluid regions[25], the porous-structure region Γ_{STR} boundary condition is given by:

$$\frac{\partial\phi^f_{STR}}{\partial n} = -\varepsilon\frac{\partial\phi^s_{STR}}{\partial n}$$
$$\text{and } \phi^f_{STR} = (S+if)\phi^f_{STR} \quad \ldots (4)$$

The structure is assumed to be situated between the two auxiliary boundaries Γ_{INPUT} and Γ_{OUTPUT} on each side. Consequently, for input and output open boundary conditions, the far-field radiation condition is given by:

$$\lim_{n\to\infty}\sqrt{r}\left(\frac{\partial\phi}{\partial r} - ik\phi\right) = 0 \quad \ldots (5)$$

Where, $r = \sqrt{x^2+y^2}$. The velocity potential function at the input and output boundaries can be expressed as:

$$\begin{cases}\phi_{Input} = \phi_I + \phi_R, \\ \phi_{Output} = \phi_T, \end{cases} \quad \ldots (6)$$

Considering the principle of small-amplitude waves, the velocity potential functions can be written as:

$$\phi_{Input} = \frac{iag}{\omega}\left[I_0e^{ikx} + R_0e^{-ikx}\right]f_0(y), \text{ as } x \to \infty,$$
$$\phi_{Output} = \frac{iag}{\omega}\left[T_0e^{ikx}\right]f_0(y), \text{ as } x \to -\infty, \quad \ldots (7)$$

Where, the function $f_0(y)$ is given by

$$f_0(y) = \frac{\cosh k(h+y)}{\cosh kh} \quad \ldots (8)$$

The wave number k and the angular wave frequency ω satisfy the dispersion relation

$$\omega^2 = gk\tanh k \quad \ldots (9)$$

The solution approach for the dual H-shaped breakwater is discussed in detail in the next subsection.

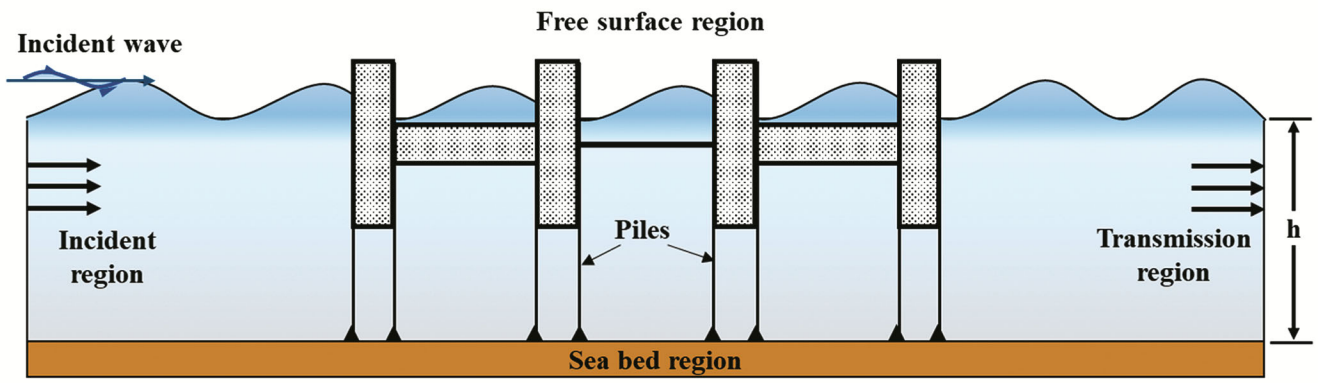

Fig. 1 — Schematic diagram of dual H-shaped breakwater

Method of solution using multi-domain boundary element method

The wave interaction with pile-restrained dual H-shaped breakwaters is analysed using the MDBEM approach. The general field point and the source point comprise the current computational domain. In Figure 2, a brief narrative of the boundaries for fluid and structural region and fluid-structure interfaces is presented in detail. The fundamental solution of the governing equation is provided as:

$$\nabla^2 G - {k_z}^2 G = \delta(\xi - x, \eta - y) \quad \ldots (10)$$

Where, G is expressed as:

$$G(x, y, \xi, \eta) = \frac{-K_0(k_z r)}{2\pi} \quad \ldots (11)$$

Where, $r = \sqrt{(x-\xi)^2 + (y-\eta)^2}$ referred to as the distance between the source point $Q(\xi, \eta)$ and the field point $P(x, y)$, where $Q(\xi, \eta)$. The second-kind modified zeroth-order Bessel function is denoted by K_0. The following equation represents the normal derivative of Green's function as:

$$\frac{\partial G}{\partial n} = \frac{k_z}{2\pi} K_1(k_z r) \frac{\partial r}{\partial n} \quad \ldots (12)$$

Where, K_1 has been referred to as a second-kind modified first-order Bessel function, and in the case of singularity $r \to 0$, the asymptotic behaviour of K_0 is given by

$$K_0(k_z r) = -\gamma - ln\left(\frac{k_z r}{2}\right) \quad \ldots (13)$$

Where, $\gamma = 0.5772$ is the Euler's constant. Further in the case of normal incident wave angle, *i.e.*, when $\theta = 0, K_0(k_z r)$ approaches $-ln(r)$.

The generalised form of the boundary integral equation, which applies Green's second identity and considers Green's function in free space, is shown as:

$$c(P)\phi(P) + \int_\Gamma \phi \frac{\partial G}{\partial n} d\Gamma = \int_\Gamma G \frac{\partial \phi}{\partial n} d\Gamma \quad \ldots (14)$$

with $c(P)$ is denoted by:

$$c(P) = \begin{cases} 1 \text{ if P} \in \Omega, \\ \frac{1}{2} \text{ if P} \in \Gamma \text{ is smooth}, \\ 0 \text{ if P} \in \Omega, \Gamma, \end{cases} \quad \ldots (15)$$

The computational domain boundary in the above equation is indicated by Γ. The final boundary integral equation can, therefore, be expressed as:

$$\frac{\phi(P)}{2} + \int_\Gamma \frac{\partial G}{\partial n} \phi \, d\Gamma = \int_\Gamma \frac{\partial \phi}{\partial n} G \, d\Gamma \quad \ldots (16)$$

The value of ϕ is assumed to be equal at the mid-element node and is regarded constant across the N constant elements that make up the boundary. Equation (16) is discretised into N constant boundary elements (Fig. 2). The discretised boundary integral equation can therefore be written as:

$$\frac{\phi(P)}{2} + \sum_{j=1}^{N} \left(\int_{\Gamma_j} \frac{\partial G}{\partial n} \phi_j \, d\Gamma \right) = \sum_{j=1}^{N} \left(\int_{\Gamma_j} \frac{\partial \phi}{\partial n} \mathrm{G}_j \, d\Gamma \right) \quad \ldots (17)$$

Where, Γ_j denoted as the j^{th} element boundary.

The expression for the boundary integral equation considering $\int_{\Gamma_j} \frac{\partial G}{\partial n} d\Gamma = H_{ij}$ and $\int_{\Gamma_j} G_j \, d\Gamma = Q_{ij}$ as in Eq. (14) is given by:

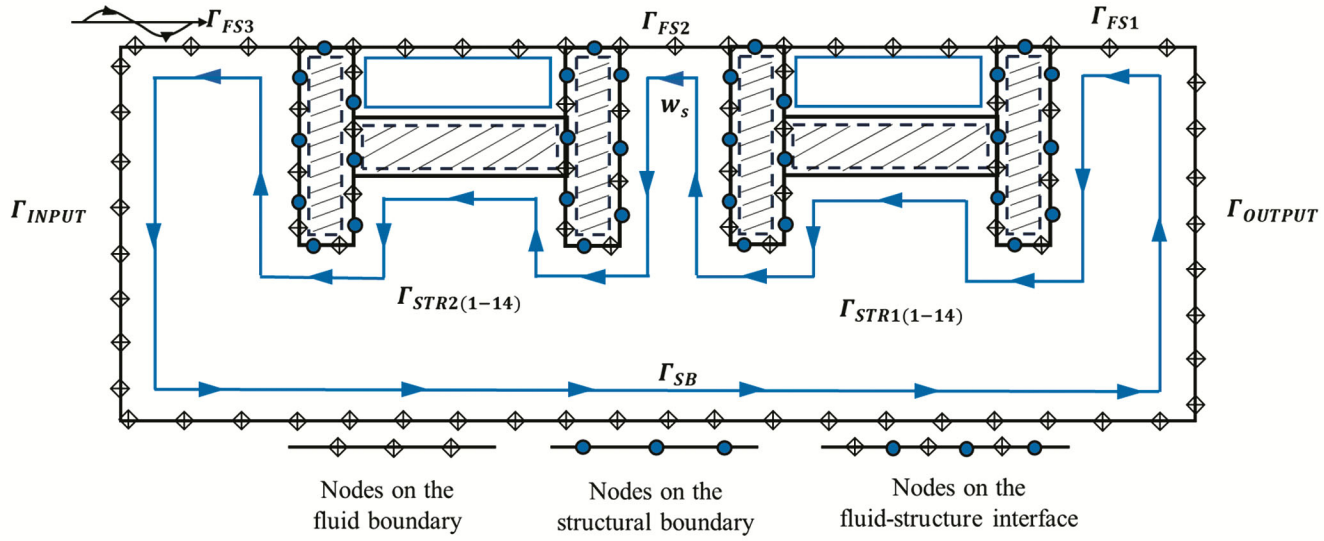

Fig. 2 — Schematic diagram representing the boundary elements for dual H-shaped breakwater

$$-\frac{\phi(P)}{2}+\sum_{j=1}^{N}\left(H_{ij}\,\phi_j\right)=\sum_{j=1}^{N}\left(Q_{ij}\frac{\partial\phi}{\partial n}\right) \quad \ldots (18)$$

The influence functions are represented by the integrals H_{ij} and G_{ij} between the element i at which the fundamental solution is applied and another element j under consideration[24]. When the breakwater zones interact with the sea bottom, free surface, and fluid regions, the corresponding physical characteristics and dimensions are replaced in the boundary conditions, and the enlarged discretised equation can be presented as:

$$-\frac{1}{2}\phi^{f_R}+\sum_{j=1}^{N}\left(H_{ij}\phi_{SB}^{f}\right)+\sum_{j=1}^{N}\left(H_{ij}-ikQ_{ij}\right)\phi_{OUTPUT}^{f}+\sum_{j=1}^{N}\left(H_{ij}-\frac{\omega^2}{g}Q_{ij}\right)\phi_{FS1}^{f}+\sum_{j=1}^{N}\left(H_{ij}\phi_{STR1}^{f}\right)-\sum_{j=1}^{N}\left(Q_{ij}\frac{\partial\phi_{STR1}^{f}}{\partial n}\right)+\sum_{j=1}^{N}\left(H_{ij}-\frac{\omega^2}{g}Q_{ij}\right)\phi_{FS2}^{f}+\sum_{j=1}^{N}\left(H_{ij}\phi_{STR2}^{f}\right)+\sum_{j=1}^{N}\left(H_{ij}\phi_{STR1}^{f}\right)-\sum_{j=1}^{N}\left(Q_{ij}\frac{\partial\phi_{STR1}^{f}}{\partial n}\right)+\sum_{j=1}^{N}\left(H_{ij}-\frac{\omega^2}{g}Q_{ij}\right)\phi_{FS2}^{f}+\sum_{j=1}^{N}\left(H_{ij}\phi_{STR2}^{f}\right)+\sum_{j=1}^{N}\left(H_{ij}\phi_{STR1}^{f}\right)-\sum_{j=1}^{N}\left(Q_{ij}\frac{\partial\phi_{STR1}^{f}}{\partial n}\right)+\sum_{j=1}^{N}\left(H_{ij}-\frac{\omega^2}{g}Q_{ij}\right)\phi_{FS2}^{f}+\sum_{j=1}^{N}\left(H_{ij}\phi_{STR2}^{f}\right)-\sum_{j=1}^{N}\left(Q_{ij}\frac{\partial\phi_{STR2}^{f}}{\partial n}\right)+\sum_{j=1}^{N}\left(H_{ij}-\frac{\omega^2}{g}Q_{ij}\right)\phi_{FS3}^{f}+\sum_{j=1}^{N}\left(H_{ij}-ikQ_{ij}\right)\phi_{INPUT}^{f}=0 \quad \ldots (19)$$

The discretised equations for the leeside and seaside breakwaters considering structural region boundary conditions are given by:

$$-\frac{1}{2}\phi^{s}+\sum_{j=1}^{N}\left(H_{ij}\phi_{STR1}^{s}\right)-\sum_{j=1}^{N}\left(Q_{ij}\frac{\partial\phi_{STR1}^{s}}{\partial n}\right)=0 \quad \ldots (20)$$

$$-\frac{1}{2}\phi^{s}+\sum_{j=1}^{N}\left(H_{ij}\phi_{STR2}^{s}\right)-\sum_{j=1}^{N}\left(Q_{ij}\frac{\partial\phi_{STR2}^{s}}{\partial n}\right)=0 \quad \ldots (21)$$

For the fluid region (indicated as superscripts f) and structural region (indicated as superscripts s), the updated discretised equation for replacing the input and output velocity potentials in Eq. (7) can be expressed as:

$$-\frac{1}{2}\phi^{f_R}+\sum_{j=1}^{N}\left(H_{ij}\phi_{SB}^{f}\right)+\sum_{j=1}^{N}\left(H_{ij}-ikQ_{ij}\right)\phi_{T}^{f}+\sum_{j=1}^{N}\left(H_{ij}-\frac{\omega^2}{g}Q_{ij}\right)\phi_{FS1}^{f}+\sum_{j=1}^{N}\left(H_{ij}\phi_{STR1}^{f}\right)-\sum_{j=1}^{N}\left(Q_{ij}\frac{\partial\phi_{STR1}^{f}}{\partial n}\right)+\sum_{j=1}^{N}\left(H_{ij}-\frac{\omega^2}{g}Q_{ij}\right)\phi_{FS2}^{f}+\sum_{j=1}^{N}\left(H_{ij}\phi_{STR2}^{f}\right)-\sum_{j=1}^{N}\left(Q_{ij}\frac{\partial\phi_{STR2}^{f}}{\partial n}\right)+\sum_{j=1}^{N}\left(H_{ij}-\frac{\omega^2}{g}Q_{ij}\right)\phi_{FS3}^{f}+\sum_{j=1}^{N}\left(H_{ij}-ikQ_{ij}\right)\phi_{R}^{f}=-\sum_{j=1}^{N}\left(H_{ij}-ikQ_{ij}\right)\phi_{I}^{f} \quad \ldots (22)$$

The interface boundaries for both fluid and structure regions have the same potential φ_{STRj}^{m} and flux $\frac{\partial\varphi_{STRj}^{m}}{\partial n}$ on the boundary. It is assumed that the structure-seabed interface and structure-free surface interface are rigid. So, the flux is given by:

$$\frac{\partial\varphi_{STRj}^{m}}{\partial n}=0 \quad \ldots (23)$$

Further, the matching boundary conditions are applied to obtain the unknown potentials ϕ_I , ϕ_R and ϕ_T to solve the system of linear equations using the Gauss-elimination technique. The hydrodynamic coefficients are calculated using the relations

$$K_r=\left|\frac{R_0}{I_0}\right|, K_t=\left|\frac{T_0}{I_0}\right| \; and \; K_d=\sqrt{1-K_r^2-K_t^2} \quad \ldots (24)$$

The relation that determines the horizontal and vertical wave forces operating on the structure can be expressed as:

$$F_x=Re\left[i\rho\omega\int_{\Gamma_{STR_j}}\{n_x\}\,\phi_{STR}\,d\Gamma\right] \quad \ldots (25)$$

Where, n_x is the unit normal vectors in x-direction on Γ_{STR} and the coefficient for wave force can be expressed as: $K_{Fx}=\frac{F_x}{i\rho\omega}$

Numerical Results and Discussion

This research employs a numerical investigation to evaluate the hydrodynamic behaviour of dual pile-restrained, H-shaped floating breakwaters based on the MDBEM approach. The reflection, transmission, dissipation coefficient, and wave force coefficients are examined for the angle of wave incidence, on varying the structural parameters of the breakwaters, such as their relative draft and width. MATLAB is used for the numerical analysis, and the simulation results are compared with the results that have been published in the literature.

Convergence of boundary element for a dual H-shaped breakwater

Table 1 displays the convergence of the developed MDBEM technique in terms of the reflection and transmission coefficients K_r and K_t respectively for

Table 1 — Convergence of K_r and K_t with the increment of boundary elements

Γ_{SB}	Γ_O	Γ_{FS_1}	$\Gamma_{STR1_{1-14}}$	Γ_{FS_2}	$\Gamma_{STR2_{1-14}}$	Γ_{FS_3}	Γ_I	Δx	N	K_r	K_t
66	10	10	24	10	24	10	10	0.1	164	0.647128	0.017210
132	20	20	48	20	48	20	20	0.05	328	0.647259	0.017689
660	100	100	240	100	240	100	100	0.01	1640	0.647612	0.017882
1320	200	200	480	200	480	200	200	0.005	3280	0.647665	0.017904

the wave interaction with dual H-shaped breakwaters with $\theta = 0^0$. As seen in Figure 2, the boundary is discretised into N a number of elements. The convergence of K_r and K_t is noted up to four decimal places for the constant element length $\Delta x = 0.01$ and $\Delta x = 0.005$. In the present study, the constant element length $\Delta x = 0.01$ is taken into consideration to analyse the structural characteristics. The boundary surface is discretised with elements of size 1/100th at each 1 m of boundary length.

Validation of the present nnumerical model

The wave interaction with dual floating porous boxes validates the numerical analysis conducted using the MDBEM technique proposed by Vijay & Sahoo[22] as depicted in Figure 3. The structural parameters considered for the study are the relative thickness $\delta/h = 0.02$, force resistance coefficient $f = 9.03$, draft-to-width ratio $d/b = 0.50$, relative spacing $L/h = 0.50$, relative draft $h/d = 4.0$, porosity $\mu = 0.15$, inertia force coefficient $s = 2.93$, and the complex porous effect parameter $G_s = 0.75 + 0.24i$.

The study indicates that due to the energy dissipation and reflection properties, the seaside structure receives a force that is noticeably higher than that of the leeside structure. The two porous boxes efficiently absorb some of the wave energy on the leeside, which helps to reduce the height of the waves. The numerical study shows a satisfactory validation in Figure 3 using the MDBEM approach with the result obtained by Vijay & Sahoo[22]; hence, the MDBEM approach is employed to study the performance of dual H-shaped breakwaters restrained by piles.

Based on the Multi-Domain Boundary Element Methodology (MDBEM), the numerical analysis offers an additional deterministic method that incorporates the boundary elements on the domain boundaries. The MDBEM technique makes the numerical computation simpler and more efficient by discretising the boundaries. Furthermore, with a substantially shorter execution time, the MDBEM technique presents extremely accurate and appropriate solutions for open-boundary scenarios. Furthermore, a more thorough examination of multi-domain borders that takes fluid and heterogeneous structural boundaries into account is possible through the combination of the MDBEM technique with additional analytical and numerical tools.

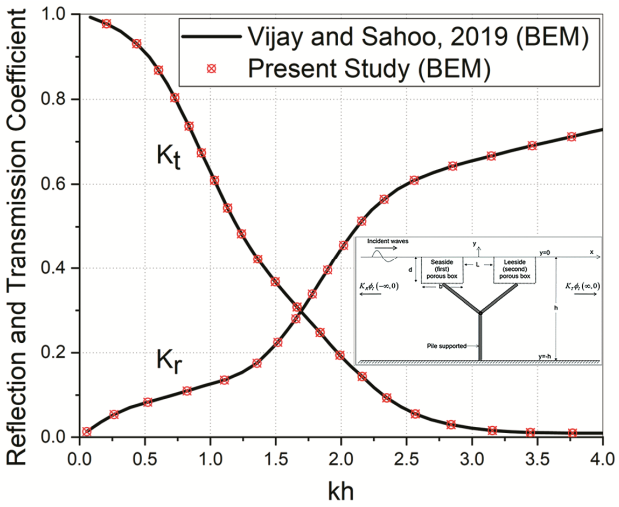

Fig. 3 — Comparative study of K_r and K_t for a pair of floating porous boxes using MDBEM approach (Vijay & Sahoo[22])

Reflection, transmission and dissipation coefficients

The wave transformation near offshore structures contributes to an important study for assessing their performance and preserving structural integrity. Understanding the reflection behaviour of a breakwater while interacting with the incoming wave is crucial to countering wave attenuation and energy dissipation and designing an effective offshore structure. Analysing the reflection and transmission behaviour under different conditions of structural and physical properties provides a perspective of a suitable shape and dimensions of the breakwater for effective installation. Investigating the effect of incoming wave-induced force on the breakwater surface is the prime task for studying structural instability and integrity. The present study analyses the possible structural parameters for a pair of H-shaped breakwaters on varying angles of incidence θ. The modelled structures are considered porous with the geometrical parameters of $\varepsilon_w = 0.1$, $\varepsilon_f = 0.2, f_f = 1.2$ $f_f = 1.0$ and $S_w = S_f = 1$.

Effect of changing submergence draft of the web

The variation of hydrodynamic coefficients K_r, K_t and K_d versus wave incident angles θ for different web submergence drafts varying within $0.3 \leq d_w/h \leq 0.6$ is presented in Figure 4(a,b). The oscillatory patterns observed in the hydrodynamic coefficients are may be due to structural spacing between the breakwaters[22]. The reflection coefficient (Fig. 4a) is noted higher for the higher draft at $\theta \leq 30^0$, and it follows an opposite pattern for $\theta \geq 50^0$. The dual H-shaped breakwater system dissipates lower wave energy within the critical range, as shown in Figure 4(b). The sudden increase in K_r observed between $30^0 \leq \theta \leq 50^0$ can be referred to as the critical angle range to attain higher reflected and transmitted waves. The web acts as a vertical barrier and promotes wave reflection. Hence, increasing the web draft leads to incrementing the surface area for wave reflection, which is observed for $\theta \leq 30^0$. The wave reflection is around 1.13 times higher when the web draft is doubled for $30^0 \leq \theta \leq 50^0$. As the incident angle increases and is around $\theta \geq 50^0$, the incident wave is nearly parallel to the breakwater, causing a reduction in wave reflection for higher web draft. The transmission is less for a higher draft and is maximum in the critical angle range.

Effect of changing the width of the web

The variation in K_r, K_t and K_d versus wave incident angles θ for different widths of the web varying within $0.1 \leq b_w/h \leq 0.4$ is illustrated in Figure 5(a,b). The

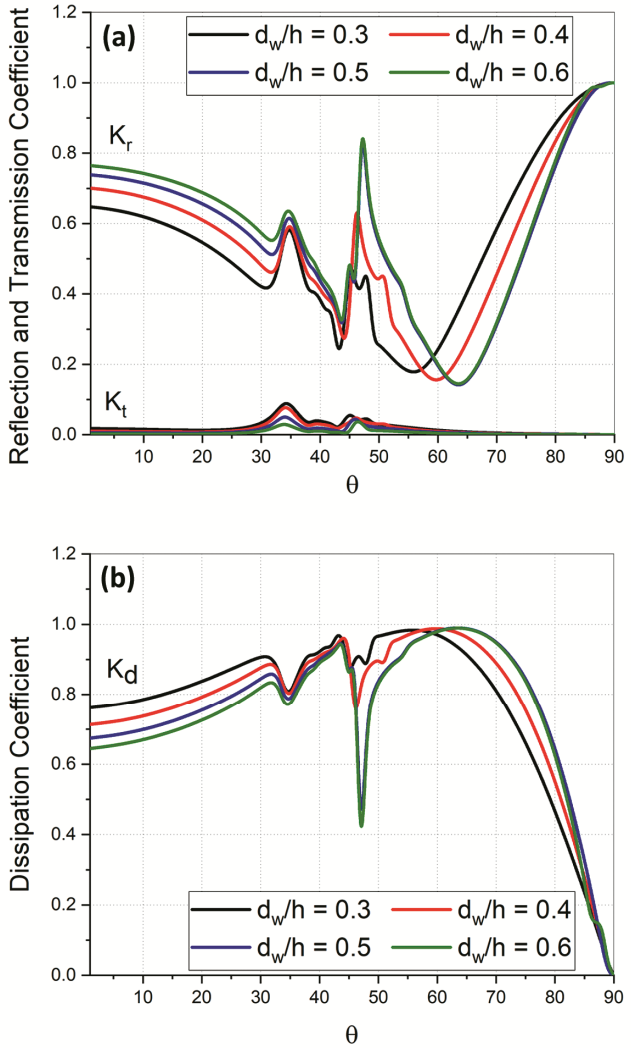

Fig. 4 — Variation of (a) K_r and K_t; and (b) K_d versus θ for different width of web d_w/h for single H-shaped breakwater having $b_w/h = 0.1$ and $b_f/h = 1.6$

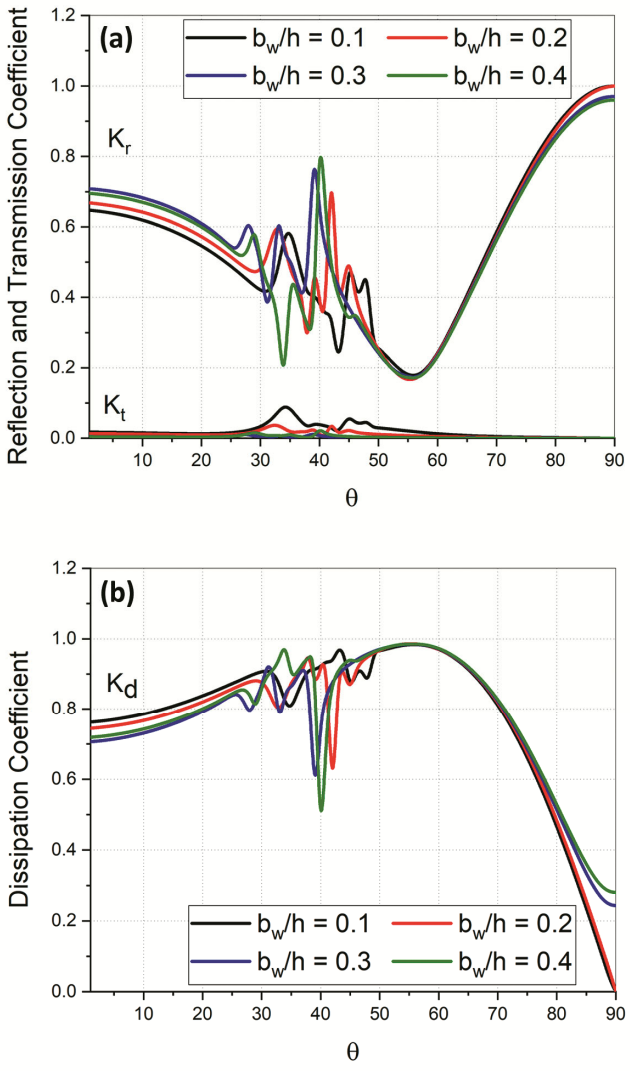

Fig. 5 — Variation of (a) K_r and K_t; and (b) K_d versus θ for different width of web b_w/h for single H-shaped breakwater having $d_w/h = 0.3$ and $b_f/h = 1.6$

spacing between the adjacent structures causes oscillatory trends and spikes in specific intervals of wave incident angles. In the case of a lower value of wave incidence $\theta \leq 30^0$, increasing web width apparently enhances the damping in wave energy due to the larger porous structure volume throughout the structure observed in Figure 5(a). The observed critical incident angle range is within $30^0 \leq \theta \leq 50^0$ having oscillatory variations and spikes as the structural spacing within the flanges causes wave trapping. A similar observation for energy dissipation characteristics is noted in Figure 5(b). The least energy of 50 % is dissipated by the widest web, where it reflects a higher energy of 80 % for the incidence value under the critical angle range. The narrower web transmits higher energy within the range and additional design considerations must be adapted for efficient performance.

Effect of changing the width of the flange

The variation of K_r, K_t and K_d versus wave incident angles θ are shown in Figure 6(a,b) for different widths of flange varying within $1.6 \leq b_f/h \leq 2.4$. The effect of varying flange width of the H-shaped structures is negligible; however, an oscillatory pattern is observed within $25^0 \leq \theta \leq 50^0$.

The flange in an H-shaped structure provides space for water mass, which results in a significant amount of wave trapping, causing higher reflection and lower transmission. In the critical angle range, the breakwaters attain a higher reflection of around 75 % for the widest flange of $b_f/h = 2.4$ compared to other cases due to the combined effect of inter-structural spacing and the water mass present within the unit structure for maximum wave trapping. Increased transmission for incident angles within the range necessitates additional protective measures. According to Figure 6(a), higher reflection results at higher angles $\theta \geq 55^0$ as the wave propagating more parallel to the structure hence causes lower energy absorption in Figure 6(b).

Wave force coefficients

The wave induced forces on the interconnected dual H-shaped breakwater are analysed for variation in structural parameters such as d_w/h, b_w/h and b_f/h against wave incident angles θ. The wave force coefficients are analysed on the front face of the seaside breakwater and leeside breakwater, denoted as K_{fb1} and K_{fb2}, respectively.

Effect of changing submergence draft of web

The variation in the wave force coefficients K_{fb1} and K_{fb2}, versus wave incident angles θ for different web submergence drafts within $0.3 \leq d_w/h \leq 0.6$ is presented in Figure 7(a,b). The dual H-shaped breakwaters undergo increased force in the critical wave incident angle $30^0 \leq \theta \leq 50^0$ compared to other incident angles.

The maximum wave force attained by the deeper web is on both the seaside and leeside structures. The wave force coefficient increases with higher d_w/h because a larger surface area is accessible. The wave force acting on the leeside structure is 2.5 times more than the primary structure for the critical angle of incidences. Hence, a structure with a lesser

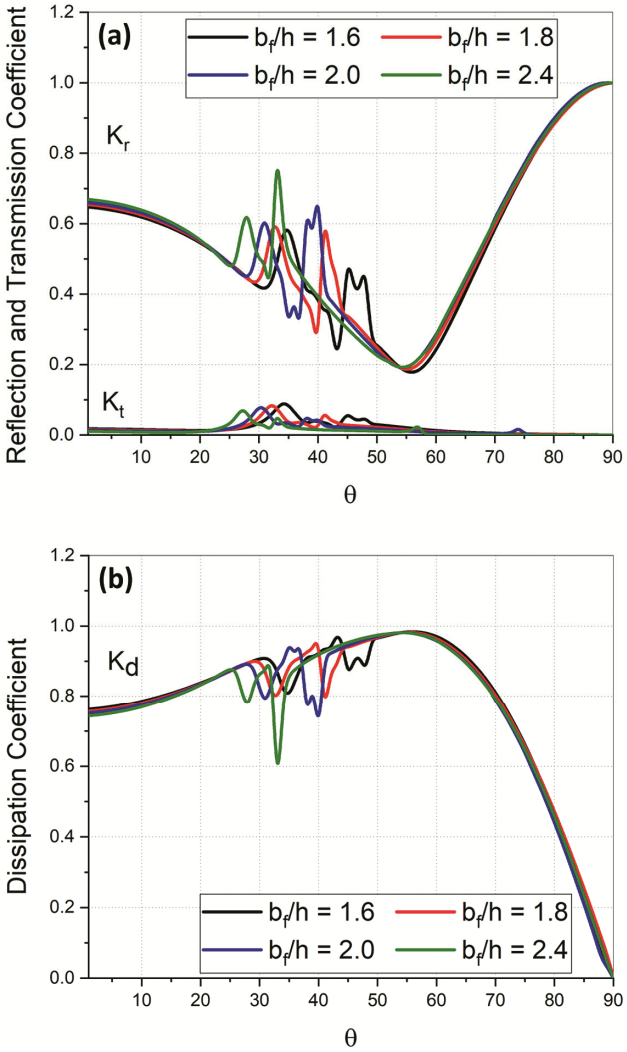

Fig. 6 — Variation of (a) K_r and K_t; and (b) K_d versus θ for different width of web b_f/h for single H-shaped breakwater having $d_w/h = 0.3$ and $b_w/h = 0.1$

submergence draft is recommended for efficient performance of specific wave incidence.

Effect of changing the width of the web

Variation of K_{fb1} and K_{fb2} versus wave incident angles θ for different widths of web varying within $0.1 \leq b_w/h \leq 0.4$ is illustrated in Figure 8(a,b). The study reveals that the secondary breakwater experiences a stronger wave attack, which may be due to phenomena such as the negative pressure generated around its surface and the intensified wave energy caused by the repeated structure that directly impacts consecutive waves within the structural spacing between the breakwaters. The secondary structure for incident angles within the critical range, particularly the web section for $b_w/h = 0.3$, experiences wave forces more than double for those acting on the primary structure. Thus, the porous structure with higher width experiences lesser impact as a significant amount of energy gets absorbed in the porous region.

Effect of changing the width of the flange

The variation of K_{fb1} and K_{fb2}, versus wave incident angles θ is illustrated in Figure 9(a,b) for different widths of flange varying within $1.6 \leq b_f/h \leq 2.4$. In Figure 9(a), the pair of H-shaped breakwaters shows an oscillatory pattern of wave force for wave incident angle $20^0 \leq \theta \leq 80^0$. The spacing between the porous structures promotes the oscillations in force coefficients. The leeside structure encounters a wave force twice the force experienced by the seaside structure, and the phenomenon is

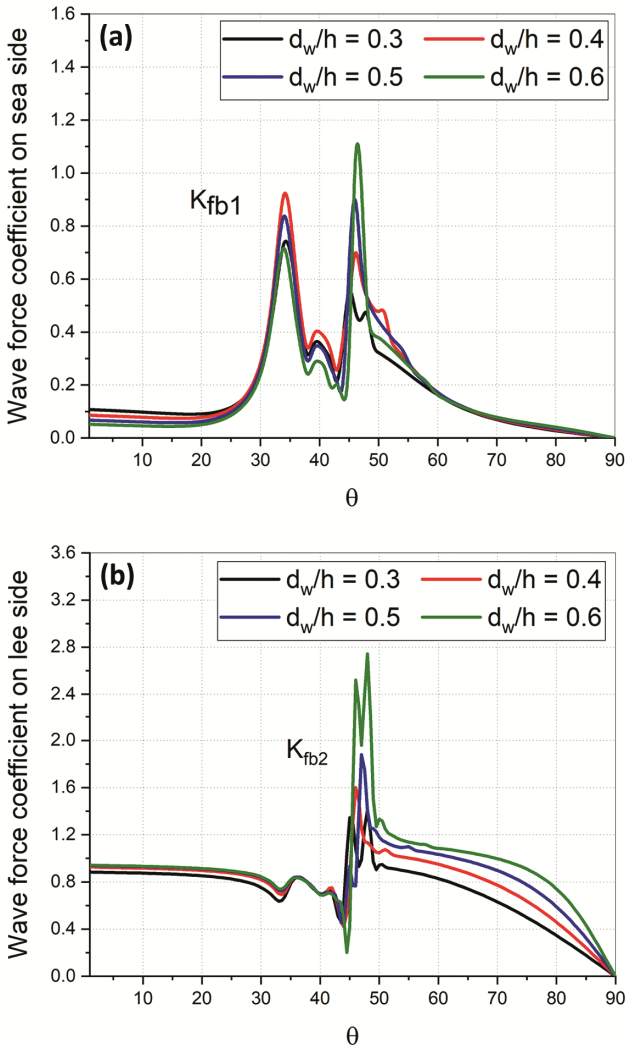

Fig. 7 — Variation of (a) K_{fb1}; and (b) K_{fb2} versus θ for different width of web d_w/h for dual H-shaped breakwater having $b_w/h = 0.1$ and $b_f/h = 1.6$

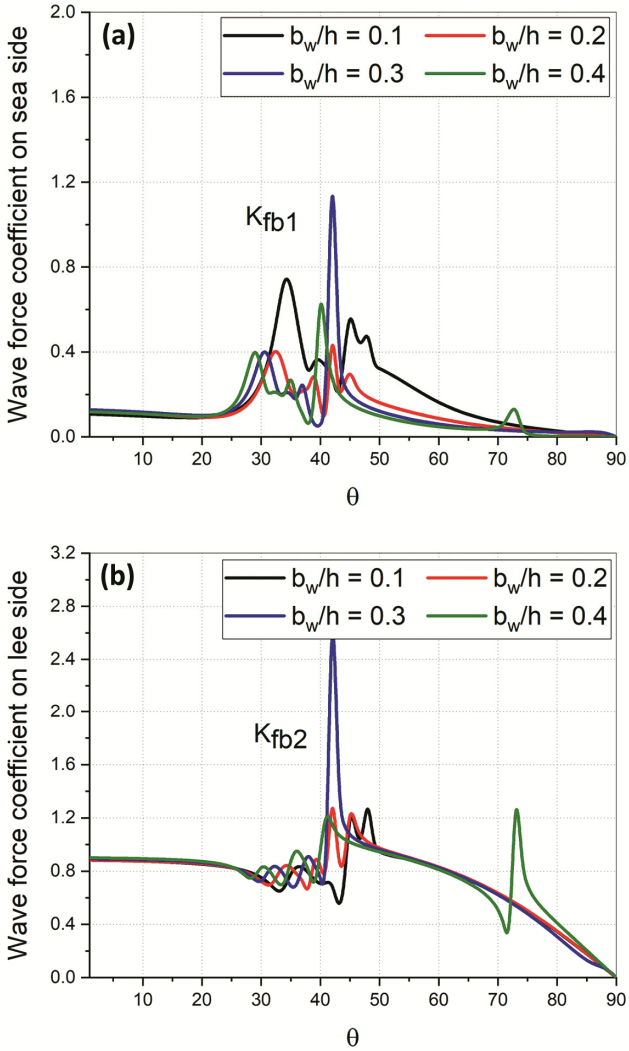

Fig. 8 — Variation of (a) K_{fb1}; and (b) K_{fb2} versus θ for different width of web b_w/h for dual H-shaped breakwater having $d_w/h = 0.3$ and $b_f/h = 1.6$

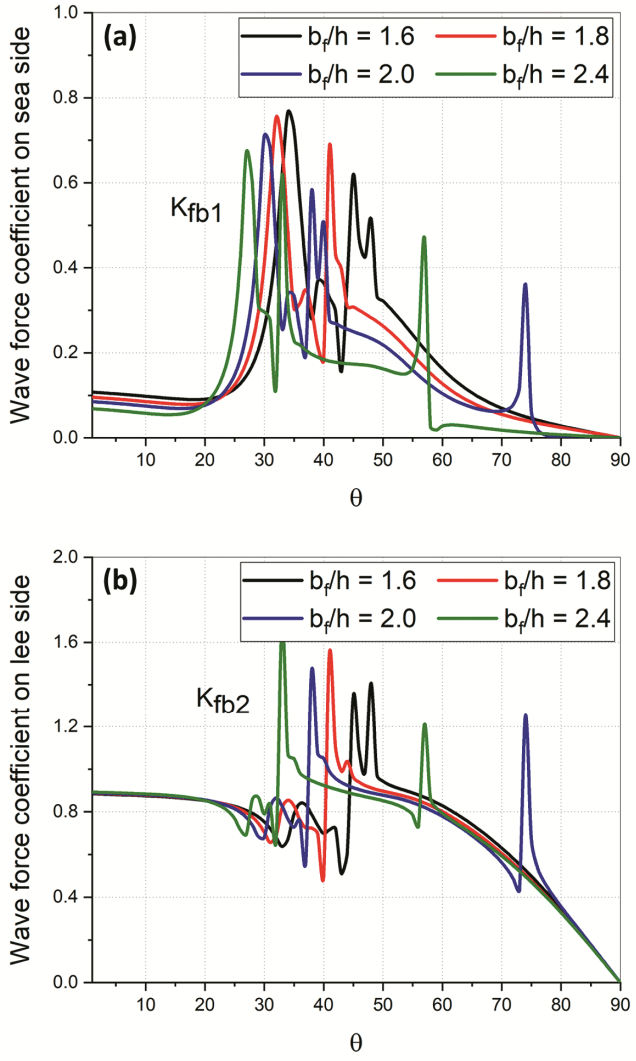

Fig. 9 — Variation of (a) K_{fb1}; and (b) K_{fb2} versus θ for different width of web b_f/h for dual H-shaped breakwater having $d_w/h = 0.3$ and $b_w/h = 0.1$

prominent within the critical incidence range. The primary reason for the least wave influence on the horizontal components of the constructions is the wave trapped between the webs, which act as vertical barriers to the incoming wave energy.

Conclusion

The study analyses the hydrodynamic performance of a multi-unit breakwater system comprised of two interconnected pile-restrained H-shaped breakwaters. The MDBEM is employed to analyse the hydrodynamic coefficients and the horizontal wave forces for various structural parameters of H-shaped breakwater, such as the width b_w and submergence draft d_w of the webs and width of a flange b_f by varying the angle of incidence. Free surface and structural interface conditions are employed with suitable edge conditions to analyse the hydrodynamic performance of the proposed dual breakwater. The established numerical results from the existing literature is compared with the results obtained through the MDBEM technique to verify the accuracy of the numerical findings. The conclusions drawn from the hydrodynamic performance of the dual H-shaped breakwaters are as follows:

- The critical angle to allow maximum transmitted energy is noted to be within $30^0 \leq \theta \leq 50^0$ for the dual H-shaped breakwaters.
- The wave reflection is observed to get doubled as the web draft is doubled within the critical angle range.
- The widest web of $b_w/h \leq 0.4$ dissipates the least wave energy of 50 % but reflects around 80 % of wave energy at critical angles.
- The breakwaters attain a higher reflection coefficient of around 75 % for the widest flange of $b_f/h = 2.4$ in the critical angle range.
- The leeside structure experiences 2.5 times more wave force compared to the primary structure for the critical angle of incidences.
- The induced wave forces on the secondary structure, especially the web section for $b_w/h = 0.3$, are more than twice as strong as those operating on the primary structure for incident angles falling within the critical range.
- The least influence on the wave interaction is caused by the wave trapped between the webs and the flange, which act as vertical barriers to the incoming wave energy.

Acknowledgements

The authors are grateful to the Ministry of Education (MoE), Government of India and the National Institute of Technology, Karnataka, Surathkal for providing the necessary facilities for pursuing the research work.

Conflict of Interest

The authors declare that they have no competing financial interests or personal relationships that could have appeared to influence the work reported in this paper.

Author Contributions

AP: Conceptualisation, methodology, validation, writing – original draft, visualisation, and investigation. DK: Conceptualization, methodology, supervision, and writing – review & editing. MR: Supervision and writing – review & editing.

References

1 Adee B H, Floating breakwater performance, In: *Coastal Engineering*, (American Society of Civil Engineers, Virginia, United States), 1976, pp. 2777-2791. https://doi.org/10.1061/9780872620834.159

2 Hales L Z, *Floating Breakwaters: State-of-the-Art Literature Review*, U.S. army, corps of engineers, coastal engineering research centre, Technical Report No. 81-1, 1981, pp. 289. https://apps.dtic.mil/sti/citations/ADA110692

3 Dai J, Wang C M, Utsunomiya T & Duan W, Review of recent research and developments on floating breakwaters, *Ocean Eng*, 158 (2018) 132–151. https://doi.org/10.1016/j.oceaneng.2018.03.083

4 Katō J, Hagino S & Uekita Y, Damping effect of floating breakwater to which anti-rolling system is applied, In: *Coastal Engineering*, (American Society of Civil Engineers, Virginia, United States), 1966, pp. 1068-1078. https://doi.org/10.1061/9780872620087.063

5 Mei C C & Black J L, Scattering of surface waves by rectangular obstacles in waters of finite depth, *J Fluid Mech*, 38 (3) (1969) 499-511. https://doi.org/10.1017/S0022112069000309

6 Dattatri J, Raman H & Shankar N J, Performance characteristics of submerged breakwaters, In: *Coastal Engineering*, (American Society of Civil Engineers, Virginia, United States), 1978, pp. 2153-2171. https://doi.org/10.1061/9780872621909.132

7 Madsen P A, Wave reflection from a vertical permeable wave absorber, *Coast Eng*, 7 (4) (1983) 381-396. https://doi.org/10.1016/0378-3839(83)90005-4

8 Abul-Azm A G & Gesraha M R, Approximation to the hydrodynamics of floating pontoons under oblique waves dual pontoon floating breakwater, *Ocean Eng*, 27 (4) (2000) 365-384. https://doi.org/10.1016/S0029-8018(98)00057-2

9 Stiassnie M & Drimer N, On a freely floating porous box in shallow water waves, *Appl Ocean Res*, 25 (5) (2003) 263-268. https://doi.org/10.1016/j.apor.2003.12.001

10 Neelamani S & Rajendran R, Wave interaction with T-type breakwaters, *Ocean Eng*, 29 (2) (2002) 151-175. https://doi.org/10.1016/S0029-8018(00)00060-3

11 Wang H Y & Sun Z C, Experimental study of a porous floating breakwater, *Ocean Eng*, 37 (5-6) (2010) 520-527. https://doi.org/10.1016/j.oceaneng.2009.12.005

12 He F, Huang Z & Law A W K, Hydrodynamic performance of a rectangular floating breakwater with and without pneumatic chambers: An experimental study, *Ocean Eng*, 51 (2012) 16–27. https://doi.org/10.1016/j.oceaneng.2012.05.008

13 Koraim A S & Rageh O S, Effect of under connected plates on the hydrodynamic efficiency of the floating breakwater, *China Ocean Eng*, 28 (2014) 349-362. https://doi.org/10.1007/s13344-014-0028-1

14 Syed S A & Mani J S, Performance of rigidly interconnected multiple floating pontoons, *J Nav Archit Mar Eng*, 1 (1) (2004) 1-15. http://aname.8m.net/jname

15 Cho Y S, Lee J I & Kim Y T, Experimental study of strong reflection of regular water waves over submerged breakwaters in tandem, *Ocean Eng*, 31 (10) (2004) 1325-1335. https://doi.org/10.1016/j.oceaneng.2003.07.009

16 Liu Y, Li H J & Zhu L, Bragg reflection of water waves by multiple submerged semi-circular breakwaters, *Applied Ocean Res*, 56 (2016) 67-78. https://doi.org/10.1016/j.apor.2016.01.008

17 Ouyang H T, Chen K H & Tsai C M, Investigation on bragg reflection of surface water waves induced by a train of fixed floating pontoon breakwaters, *Int J Nav Archit Ocean Eng*, 7 (6) (2015) 951-963. https://doi.org/10.1515/ijnaoe-2015-0066

18 Ćatipović I, Ćorak M, Alujević N & Parunov J, Dynamic analysis of an array of connected floating breakwaters, *J Mar Sci Eng*, 7 (9) (2019) 298. https://doi.org/10.3390/jmse7090298

19 Vijay K G & Sahoo T, Scattering of surface gravity waves by a pair of floating porous boxes, *J Offshore Mech Arct Eng*, 141 (5) (2019) 051803. https://doi.org/10.1115/1.4043415

20 Kar P, Sahoo T & Meylan M H, Bragg scattering of long waves by an array of floating flexible plates in the presence of multiple submerged trenches, *Phys Fluids*, 32 (9) (2020) p. 096603. https://doi.org/10.1063/5.0017930

21 Tseng I F, You C S & Tsai C C, Bragg Reflections of Oblique Water Waves by Periodic Surface-Piercing and Submerged Breakwaters, *J Mar Sci Eng*, 8 (522) (2020) 1-18. https://doi.org/10.3390/jmse8070522

22 Vijay K G, Venkateswarlu V & Nishad C S, Wave scattering by inverted trapezoidal porous boxes using dual boundary element method, *Ocean Eng*, 141 (5) (2021) 1-11. https://doi.org/10.1016/j.oceaneng.2020.108149

23 Wang G, Xie S, Yuan H, Wang R, Zhang T, *et al*., Numerical investigation of hydrodynamic characteristics of a dual floating breakwater, *Ocean Eng*, 294 (2024) p. 116728. https://doi.org/10.1016/j.oceaneng.2024.116728

24 Patil S B & Karmakar D, Hydrodynamic analysis of floating tunnel with submerged rubble mound breakwater, *Ocean Eng*, 264 (2022) p. 112460. https://doi.org/10.1016/j.oceaneng.2022.112460

25 Darlymple R A, Losada M A & Martin P A, Reflection and transmission from porous structure under oblique wave attack, *J Fluid Mech*, 224 (1991) 625-644. https://doi.org/10.1017/S0022112091001908